Gas-Assisted Laser-Metal Drilling: Theoretical Model

R. S. Patel* and M. Q. Brewster†
University of Illinois at Urbana-Champaign, Urbana, Illinois 61801

A theoretical model for gas-assisted low-power laser-metal interaction is developed. The steady-state, one-dimensional heat transfer and two-dimensional axisymmetric flow equations for the gas and molten metal regions are solved to obtain the melting front velocity. The model is based on the mechanism of gas-assisted molten metal expulsion and does not apply to situations where incident laser fluxes are high enough to produce significant vaporization at the metal surface. The times required to drill a hole in sheets of aluminum, copper, 304 stainless steel, and low-carbon steel for both argon and oxygen assist gases are obtained. In the case of oxygen-assisted drilling, the effects of change in absorptivity of the surface due to oxide formation and the difference in the melting point of the oxide and metal are considered. The competing effect of these two factors determines whether use of oxygen as an assist gas improves the process efficiency. The model is compared with experimental values of the drilling time obtained using a Nd-YAG laser, and reasonably good qualitative and quantitative agreement is found, although better quantitative agreement could be obtained by adjusting the absorptivity.

Nomenclature

a = nozzle parameter [see Eq. (26)]
f = velocity function in gas region
H = thickness of the metal sample
h = velocity function in liquid region
k = thermal conductivity
L = liquid layer thickness
L_g = characteristic length scale in gas phase
L_m = latent heat of fusion
Pr = Prandtl number
q = absorbed laser flux
r = radial coordinate
r_0 = radius of drilled hole
T = temperature
t = time
u_∞ = melting front velocity
V = velocity in Z direction
Z = axial coordinate
α = absorptivity
κ = thermal diffusivity
ν = kinematic viscosity
ρ = density

Subscripts

a = ambient condtion
b = boiling point
g = gas
L = liquid
m = melting point
ox = oxide
r = ratio
s = solid

Superscript

* = nondimensional quantity

Received Aug. 11, 1989; revision received and accepted for publication Jan. 16, 1990.

*Graduate Research Assistant, Department of Mechanical and Industrial Engineering; currently Staff Engineer, IBM East Fishkill Facility, Laser Process Technology Group, Hopewell Junction, NY.

†Associate Professor, Department of Mechanical and Industrial Engineering. Member AIAA.

Introduction

MOST metals can be melted and vaporized by absorption of the high-intensity pulse radiation of a focused laser beam. Whether material removal is dominated by melting or vaporization depends on the laser power and pulse duration.[1] For low-incident laser fluxes, of the order of 10^5–10^6 W/cm^2 or less and with long pulses (several milliseconds), melting dominates. For high-incident laser fluxes, of the order of 10^9–10^{12} W/cm^2 and with very short pulse duration ($\sim$10 ns), vaporization dominates. If the object of the process is simple material removal (as in drilling or cutting), the melting process is more efficient since the latent heat of vaporization is much higher than the latent heat of fusion for metals. In addition, if a gas jet is used to remove the molten metal as it forms, material removal can be achieved with substantially lower laser power than if vapor pressure recoil forces are relied on to expel the molten metal. This type of processing is referred to as gas-assisted molten metal expulsion (also known as melting and blowing) processing. This paper focuses on the process of gas-assisted molten metal expulsion drilling of metals. A schematic diagram of the process is shown in Fig. 1. The process of gas-assisted cutting is discussed elsewhere by Schuocker and Abel,[2] and the process of high-power interaction (including vaporization) is discussed elsewhere by Chan and Mazumder.[3]

In the low-power drilling process represented in Fig. 1 the assist gas jet provided by the nozzle influences the processing in several ways. As previously mentioned, the gas helps remove the molten metal and also protects the optics of the system by keeping metal vapors and debris away from it.

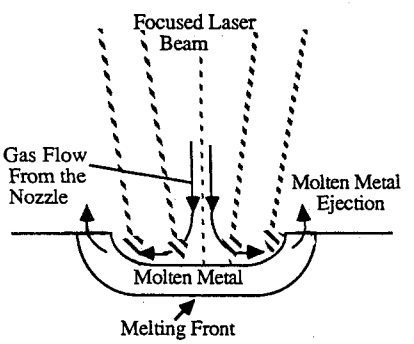

Fig. 1 Schematic diagram of gas-assisted molten metal expulsion mechanism.

Another possible effect of the gas jet is convective cooling of the surface. An additional effect of the gas jet arises when the assist gas happens to be oxygen. The heated metal reacts with oxygen, and the oxide formed can change the absorption of the incident laser beam at the surface. Also, the exothermic oxidation reaction generates additional heat at the surface. Duley and Gonsalves[4] have shown from the previously stated effects associated with the assist gas jet that during laser cutting of thin stainless steel using oxygen the rate of cooling by the gas and the rate of energy generation by exothermic oxidation are both small compared to the rate of laser energy absorption by the metal. Therefore, the potentially important factors associated with using oxygen as an assist gas that are considered in this study are 1) the change in the absorptivity during the early stages of heating due to oxide formation and 2) the difference in melting point of the oxide relative to that of the metal.

In the present model the material removal by an impinging assist gas jet has been analyzed. As the laser beam heats the metal surface, its temperature increases toward its melting point. Once the metal melts, the stagnation gas flow from the nozzle forces the metal away and expels it sideways. A balance between the rate of molten metal production at the solid-liquid interface and the radial flow rate of molten metal sheared away by the gas jet establishes a quasisteady-state situation under which the thickness of the molten metal layer remains constant and the melting front (solid-liquid interface) advances into the solid with a constant velocity. For typical metals and absorbed (not incident) laser fluxes on the order of 10^4–10^5 W/cm^2, the liquid layer is thin compared to the focused spot diameter. Under the assumption of a thin molten layer, the liquid layer thickness and interface velocity depend on the gas velocity at the nozzle exit, the laser power, and the thermophysical properties of metal and gas. The molten material removal can be modeled by assuming one-dimensional heat transfer and axisymmetric opposing stagnation flow. The mathematical formulation of this problem involves two moving boundaries: the solid-liquid interface and the liquid-gas interface. The solid-liquid interface problem has been solved as a conventional Stefan problem. The treatment of the liquid-gas interace involves solving the one-dimensional heat transfer equation to obtain the temperature distribution in the liquid phase and solving the continuity and momentum equations in the liquid and gas phases to account for the material removal due to the shearing action of gas on liquid. Since the present model is based on the gas-assisted molten metal expulsion concept, its validity requires that the vaporization rate be negligible compared to the molten metal expulsion rate. One way to guarantee this is to limit the maximum surface temperature to the boiling point of the material. If appreciable evaporation occurred, it would be necessary to account for the material removed directly by vaporization and indirectly by molten metal expulsion induced by the added recoil pressure generated because of vaporization.

Once the velocity of the melting front has been determined, this quantity is used to calculate the time required to drill a hole through a sample of a given thickness. The theoretical value of drilling time is actually calculated in two parts. First, the time required to raise the metal surface from room temperature to the melting temperature is obtained from the one-dimensional solution for a flux-heated semi-infinite solid. In the case of oxygen assist, the melting temperature of the oxide is used, and for argon assist the melting temperature of the metal is used. Second, the time taken by the melting front to reach the bottom of the sample is calculated using the melting front velocity. The total drilling time is taken to be the sum of these two times. Drilling times predicted by the model have been compared with measured drilling times for A16061 (aluminum alloy), copper, 304 stainless steel, and low-carbon steel with a Nd-YAG laser. The effect of beam power, thermophysical properties of metal, and assist gas on liquid layer thickness and drilling time are also presented and discussed.

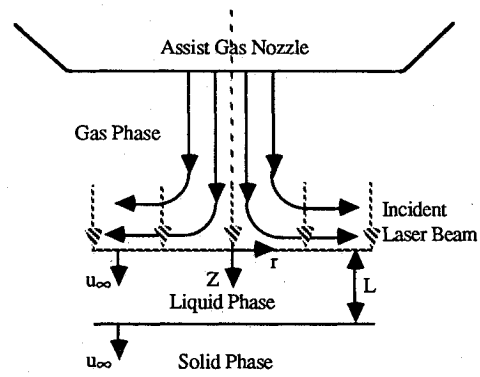

Fig. 2 Diagram of mathematical model.

Mathematical Formulation

The governing equations describing the process are derived in this section. A diagram of the model is shown in Fig 2. As the spatially uniform laser beam irradiates a target, the temperature of the target increases toward its melting point. As soon as the material melts, the assist gas jet from the nozzle, impinging on the target as a stagnation flow, shears the molten metal away in the r direction. Conduction is the dominant mode of heat transfer in both solid and liquid phases. The problem considered is basically a Stefan problem with two moving boundaries. In steady state, the thickness of the liquid layer is constant and the propagation speeds of solid-liquid and liquid-gas interfaces are the same and are referred to as the melting front velocity in the problem. The thickness of the liquid layer and the melting front velocity depend on the incident laser flux and thermophysical properties of metal and gas.

By using moving coordinates attached to the liquid-gas interface, the governing equations in nondimensional form are obtained as follows. The conduction equation in the solid phase is

$$\frac{d^2T_s^*}{dZ_s^{*2}} + \frac{dT_s^*}{dZ_s^*} = 0 \tag{1}$$

subject to the boundary conditions

$$Z_s^* = 0, \qquad T_s^* = 1 \tag{2}$$

$$Z_s^* \to \infty, \qquad T_s^* = 0 \tag{3}$$

where $T_s^* = (T_s - T_a)/(T_m - T_a)$ is the dimensionless solid temperature, and $Z_s^* = (Z-L)/(\kappa_s/u_\infty)$ is the dimensionless moving spatial coordinate in the solid phase. The conduction equation in liquid phase is

$$\frac{d^2T_L^*}{dZ_L^{*2}} = 0 \tag{4}$$

subject to the boundary conditions

$$Z_L^* = 0, \qquad \frac{dT_L^*}{dZ_L^*} = -1 \tag{5}$$

$$Z_L^* = 1, \qquad T_L^* = 0 \tag{6}$$

where $T_L^* = (T_L - T_m)/[(q/k_L)L]$ is the dimensionless liquid temperature, and $Z_L^* = Z/L$ is the dimensionless spatial variable in the liquid phase. The Stefan boundary condition at the solid-liquid interface is given as

$$u_\infty^* = -\mathrm{Ste}_f\,(\kappa_s/\kappa_L)\left.\frac{dT_L^*}{dZ_L^*}\right|_{Z_L=1} + T_m^* u_\infty^* \left.\frac{dT_s^*}{dZ_s^*}\right|_{Z_s=0} \tag{7}$$

where $u_\infty^* = (u_\infty L)/\kappa_L$ is the dimensionless drilling velocity, $T_m^* = k_s(T_m - T_a)/\rho_s L_m \kappa_s$ is the dimensionless melting temperature, and $\mathrm{Ste}_f = qL/\rho_s L_m \kappa_s$ is the Stefan number for the melting front.

The liquid phase is set into motion by the stagnation flow of an assist gas jet. Under the steady-state situation, the flow problem reduces to solving two axisymmetric opposing stagnation flows in a moving spatial coordinate system. The dimensionless forms of the momentum equations for the gas and liquid phases are

$$f^{*\prime\prime\prime} + (u_\infty^*/Pr_L v_r) f^{*\prime\prime} + 2f^* f^{*\prime\prime} - f^{*\prime 2} + L_r^{*4} = 0 \quad (8)$$

$$h^{*\prime\prime\prime} + (u_\infty^*/Pr_L) h^{*\prime\prime} + h^* h^{*\prime\prime} - h^{*\prime 2}/2 + 2\rho_r L_r^{*4} v_r^2 = 0 \quad (9)$$

subject to the coupled boundary conditions

$$Z_L^* = 0, \quad f^* = 0, \quad h^* = 0 \quad (10)$$

$$Z_L^* = 0, \quad f^{*\prime} = h^{*\prime}/2v_r, \quad f^{*\prime\prime} = h^{*\prime\prime}/2v_r^2\rho_r \quad (11)$$

$$Z_L^* \to -\infty, \quad f^{*\prime} = L_r^{*2} \quad (12)$$

$$Z_L^* = 1, \quad h^{*\prime} = 0 \quad (13)$$

where the prime denotes the differentiation with respect to Z_L^*. The quantities f^*, h^*, Pr_L, L_r^*, ρ_r, and v_r are defined as

$$f^* = f/(v_g/L)$$

$$h^* = h/(v_L/L)$$

$$Pr_L = v_L/\kappa_L$$

$$L_r^* = L/L_g$$

$$\rho_r = \rho_g/\rho_L$$

$$v_r = v_g/v_L$$

The quantity L_g is the characteristic length scale in the gas phase and is defined as

$$L_g = \sqrt{v_g/a}$$

The functions f and h are directly related to the axial velocities as given by

$$V_L(Z_L) = -h(Z_L) \quad \text{and} \quad V_g(Z_L) = -2f(Z_L) \quad (14)$$

The boundary condition in Eq. (10) ensures no penetration at the liquid-gas interface, whereas Eq. (11) ensures equal gas and liquid velocities in the r direction and also matches the shear stresses at the liquid-gas interface. The boundary condition in Eq. (12) ensures that the gas phase velocity matches the gas velocity at the nozzle exit. Finally, the boundary condition in Eq. (13) imposes the no-slip condition at the solid-liquid interface. Equating the molten metal mass flow rate generated at the solid-liquid interface over a circular area πr^2 (with arbitrary radius r) to the mass flow rate crossing the curved surface area $2\pi rL$ gives

$$u_\infty^* = Pr_L\, h^*(1) \quad (15)$$

Equations (1) and (4) can be readily solved to give

$$T_s^* = \exp(-Z_s^*) \quad (16)$$

$$T_L^* = 1 - Z_L^* \quad (17)$$

Substituting Eqs. (16) and (17) into Eq. (7) gives

$$u_\infty^* (1 + T_m^*) = \mathrm{Ste}_f(\kappa_s/\kappa_L) \quad (18)$$

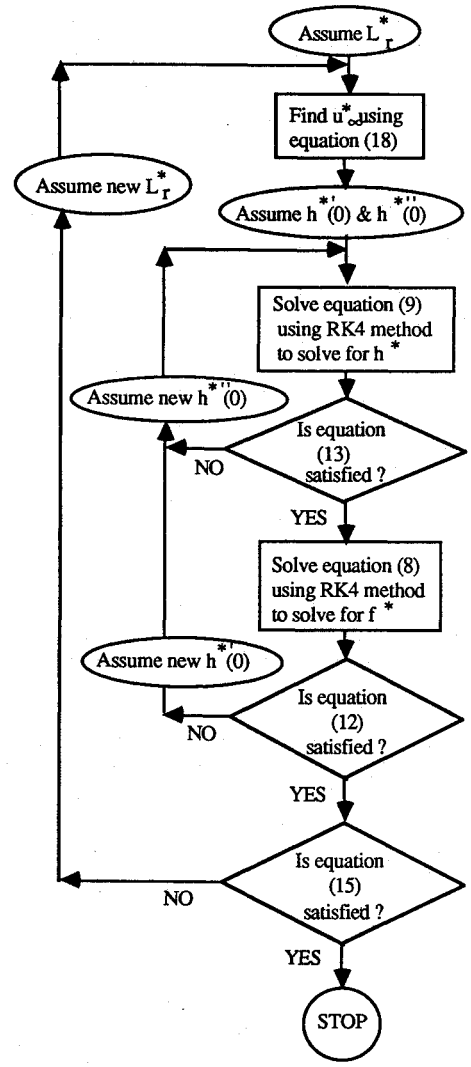

Fig. 3 Flowchart of the solution procedure.

The four unknowns of the problem are the dimensionless liquid layer thickness L_r^*, the dimensionless melting front velocity u_∞^*, the dimensionless velocity function in the gas region f^*, and the dimensionless velocity function in the liquid region h^*. The four equations used to solve for these four unknowns are Eqs. (8), (9), (15), and (18). The flowchart of the solution procedure is sketched in Fig. 3. The fourth-order Runge-Kutta (RK4) method described by White[5] has been employed to solve the nonlinear momentum equations, Eqs. (8) and (9), with coupled boundary conditions described by Eqs. (10–13).

The theoretical value of time required to drill a hole of radius r_0 into a metal sheet of thickness H is obtained as follows.

Argon Assist Case

In the case of argon-assisted laser drilling, before the metal reaches its melting temperature, the heat transfer is assumed to be governed by one-dimensional conduction with constant heat flux at the surface. This problem has a known solution given by Carslaw and Jaeger[6]:

$$T(Z,t) = \frac{2q}{k_s}\left\{\sqrt{\frac{\kappa_s t}{\pi}}\exp\left(\frac{-Z^2}{4\kappa_s t}\right) - \left(\frac{Z}{2}\right)\mathrm{erfc}\left(\frac{Z}{2\sqrt{\kappa_s t}}\right)\right\} + T_a \quad (19)$$

Therefore, the time t_1 required to reach the melting point of the metal at the surface under the influence of the absorbed

laser flux at the surface is obtained as

$$t_1 = \frac{\pi}{\kappa_s}\left\{\frac{(T_m - T_a)\,k_s}{2q}\right\}^2 \tag{20}$$

In the case of aluminum drilling using argon assist, the residual low-temperature oxide layer present on the sample surface is assumed to be too thin and weak to prevent mechanical removal of underlying molten metal. Thus, the melting point of the metal is used in Eq. (20) instead of that of the oxide. Once melting is achieved at the surface, the assist gas starts shearing the molten metal away, and quickly the steady-state problem described earlier is established. The value of drilling velocity u_∞, is used to find the time t_2 required for the melting front to reach the bottom of the sample, i.e., $Z_L = H$:

$$t_2 = (\mathrm{H} - \mathrm{L})/u_\infty \tag{21}$$

Therefore, the total theoretical drilling time is

$$t_{\mathrm{th,Ar}} = t_1 + t_2 \tag{22}$$

Oxygen Assist Case

In the case of oxygen-assisted laser drilling, the oxide formation during the early states of metal heating usually increases the laser energy absorption at the surface. But because of the presence of a relatively thick solid oxide layer, the surface will have to be heated to the oxide melting point before flow of the molten metal can occur. If the oxide melting point is significantly higher than the metal melting point, a longer heating time may be required to raise the surface to the melting temperature of the oxide. The time required to reach the melting point of the oxide at the surface under the influence of increased absorbed laser flux q_{ox} at the surface is obtained as

$$t_3 = \frac{\pi}{\kappa_s}\left\{\frac{(T_{m,\mathrm{ox}} - T_a)k_s}{2q_{\mathrm{ox}}}\right\}^2 \tag{23}$$

Once the oxide is melted, the role of oxygen then is just to shear the molten metal away, and the steady-state condition as described for the argon assist case is established. The drilling velocity u_∞ is used to find the time required for the melting front to reach the bottom of the sample:

$$t_4 = (H - L_{\mathrm{ox}} - L)/u_\infty \tag{24}$$

Table 1 Thermophysical properties of metals and oxides

	Aluminum	Copper	304 S.S.[a]	Low C steel (Fe)
T_m, K	933	1358	1700	1809
$T_{m,\mathrm{ox}}$, K	2345	1550	—	1840
T_b, K	2793	2833	—	3133
L_m, J/kg	3.88×10^5	2.05×10^5	2.7×10^5	2.72×10^5
ρ_s, kg/m^3	2700	8960	7834	7870
k_s, W/m-K	238	397	16.3	78.2
κ_s, m^2/s	0.961×10^{-4}	1.148×10^{-4}	4.438×10^{-6}	2.179×10^{-5}
ρ_L, kg/m^3	2385	8000	7015	7015
k_L, W/m-K	100	170	16.3	30
κ_L, m^2/s	3.88×10^{-5}	4.293×10^{-5}	2.923×10^{-6}	5.346×10^{-6}
ν_L, m^2/s	5.45×10^{-7}	5.0×10^{-7}	7.84×10^{-7}	7.84×10^{-7}

[a]S.S., stainless steel.

Table 2 Thermophysical properties of gases and nozzle parameter

	Argon	Oxygen
ρ_g, kg/m^3	1.784	1.429
ν_g, m^2/s	1.272×10^{-5}	1.448×10^{-5}
γ	1.658	1.395
T_0,K	300	300
R, J/kg-K	208.15	259.82
V_e, m/s	279.112	301.333
a, l/s	279,112	301,333

where L_{ox} is the location of the melting front at time t_3. The location of the melting front L_{ox} can be obtained from Eq. (19) by substituting $T = T_m$ of metal, $q = q_{\mathrm{ox}}$, and $t = t_3$ to give $Z = L_{\mathrm{ox}}$. Therefore, total theoretical drilling time under oxygen assist case is

$$t_{\mathrm{th,O_2}} = t_3 + t_4 \tag{25}$$

Results and Discussion

Solutions are obtained for aluminum, copper, 304 stainless steel, and low-carbon steel. The thermophysical properties in the solid and liquid phases, obtained from *Smithells Metals Reference Book*,[7] are given in Table 1. In the case of 304 stainless steel and low-carbon steel, the value of properties that were not readily available in the literature are approximated by the respective properties of iron.

The nozzle parameter a is calculated from

$$a = V_e/2y \tag{26}$$

where V_e is the gas velocity at the exit plane of the nozzle, and y is the distance between the nozzle exit and the metal surface (y = 0.5 mm for the present study). The gas velocity at the exit plane of a choked nozzle is calculated using

$$V_e = \sqrt{2\gamma RT_0/(\gamma + 1)} \tag{27}$$

as described by Zucrow and Hoffman,[8] where T_0 is the stagnation temperature of the gas at the nozzle inlet, R is the gas constant, and γ is the ratio of specific heats of the gas. The thermophysical properties of the assist gas and the nozzle parameter used in the calculations are given in Table 2.

Liquid Layer Thickness

The change in the liquid layer thickness as a function of the absorbed laser flux for aluminum and copper is shown in Fig. 4. For both metals the liquid layer thickness increases as the absorbed flux increases. Because of the lower dynamic viscosity of oxygen gas compared to argon gas, the liquid layer thickness when oxygen is used as an assist gas is slightly higher than that when argon is used. Also, the liquid layer thickness for copper is smaller than that of aluminum at a given absorbed laser flux because of the higher thermal conductivity of copper compared to aluminum.

Surface Temperature

The effect of absorbed laser flux on surface temperature under steady-state conditions for aluminum and copper is plotted in Fig. 5. For both metals the surface temperature

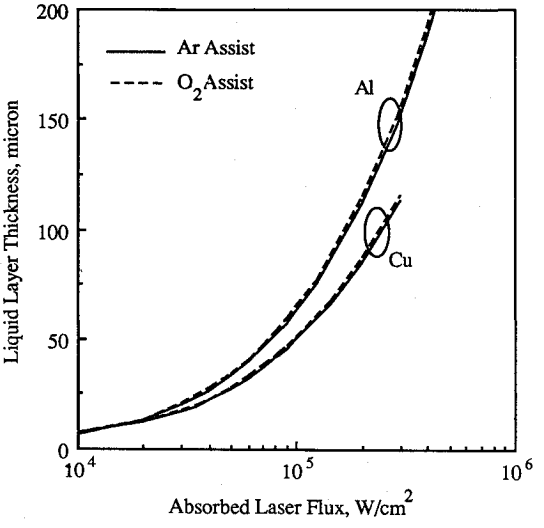

Fig. 4 Liquid layer thickness vs absorbed laser flux.

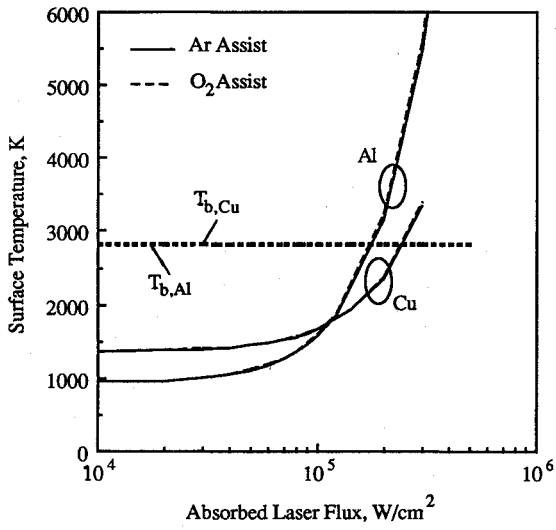

Fig. 5 Surface temperature vs absorbed laser flux.

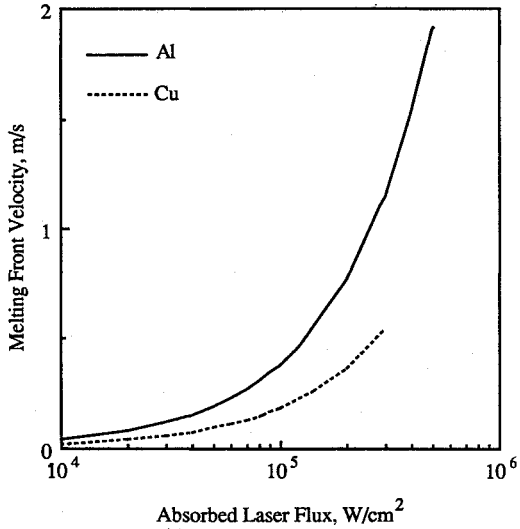

Fig. 6 Melting front velocity vs absorbed laser flux.

increases as the absorbed laser flux increases. The lower thermal conductivity of liquid aluminum compared to liquid copper results in a steeper change in temperature for aluminum. It can be seen that, in the case of aluminum for absorbed laser fluxes higher than about 2×10^5 w/cm^2, the surface temperature exceeds the boiling point of aluminum. Thus, the present model calculates the upper limit of the absorbed laser flux up to which the gas-assisted molten metal expulsion mechanism is valid. The corresponding limit for copper is 2×10^5 W/cm^2. Figure 5 also shows that for a given absorbed laser flux the difference in surface temperatures for argon and oxygen is very small. This can be attributed to the small difference in the liquid layer thickness for the two gases.

Melting Front Velocity

The change in the melting front velocity as a function of the absorbed laser flux is shown in Fig. 6. An increase in absorbed laser flux results in an increase in the melting front velocity. For a metal sheet of a given thickness, an increase in melting front velocity results in a decrease in drilling time. The higher value of velocity for aluminum compared to copper for a given absorbed laser flux is again due to the difference in the thermal properties of the two metals.

Temperature Distribution

The steady-state temperature field as a function of depth for a given absorbed laser flux is plotted in Fig. 7. The temperature within the liquid phase decreases linearly from the surface temperature to the melting temperature at the solid-liquid interface. Below the solid-liquid interface in the solid phase, the temperature exponentially decreases to the ambient temperature. The discontinuity in the temperature gradient that is due to the latent heat of fusion and change in thermal conductivities along the solid-liquid interface can be clearly observed.

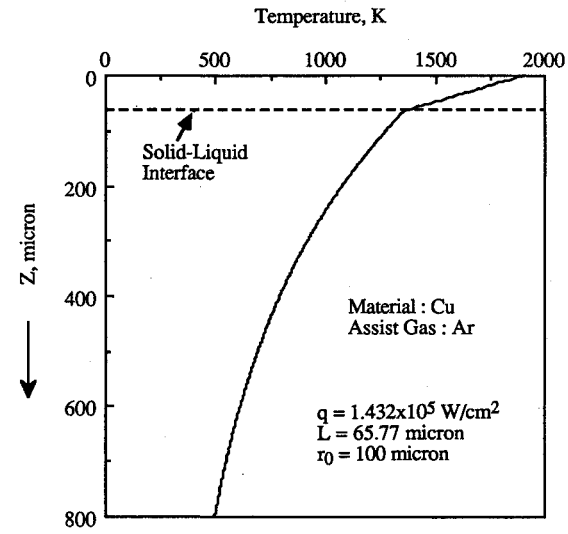

Fig. 7 Temperature profile in target material.

Drilling Time Comparison

A 100-W average power pulsed Nd-YAG laser was used to drill a hole in Al6061 (aluminum alloy), copper, 304 stainless steel sheets of thickness 1/32 in. (0.794 mm) and low-carbon steel sheet of thickness 1/16 in. (1.588 mm). A square power pulse shape with a "top hat" spatial profile was used. A coaxial nozzle (1 mm diam) placed 0.5 mm above the metal surface was used to supply an assist gas. The experimental values of drilling times were obtained for three different incident laser power levels using argon and oxygen gases. Further details of the experimental work can be found in the authors' companion study.[9] For theoretical calculation of drilling time, the values of absorbed laser flux were obtained as follows.

Argon Assist Case

The room temperature values of the normal absorptivity at 1.06 μm for Al6061, Cu, 304 stainless steel, and low-carbon steel samples studied were measured using an integrating sphere and are listed in Table 3. Therefore, t_1 and t_2 were calculated based on the amount of absorbed laser flux obtained by using the previously mentioned room temperature values of absorptivity (listed under argon assist case in Table 3).

Oxygen Assist Case

As mentioned earlier, the oxide formation during oxygen-assisted laser material processing changes the absorptivity of the surface. Accordingly, during the period of heating the metal from room temperature to the melting temperature of the oxide, values of normal absorptivity at 1.06 μm more representative of oxidized metal were used, as indicated in

Table 3 Target absorptivity

Metal	Argon assist case	Oxygen assist case
Al6061	0.28	0.4
Cu	0.02	0.2
304 Stainless steel	0.32	0.32
Low C steel	0.45	0.6

Table 3. The values listed in Table 3 were estimated based on the authors' earlier work,[10] where the effect of oxidation and plume formation on laser energy coupling with the metal were studied through reflectivity measurements, using an integrating sphere. The value of 0.6 (for the oxygen assist case) for low-carbon steel was estimated from Ref. 11. To calculate t_3, the values of absorptivity listed in Table 3 for oxygen assist case were used. To calculate t_4, the values of absorptivity listed in Table 3 for the argon assist case were used.

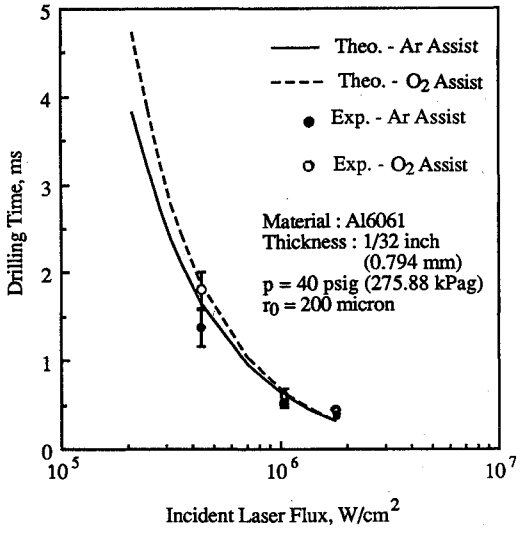

Fig. 8 Drilling time for 1/32-in. (0.794-mm) Al6061.

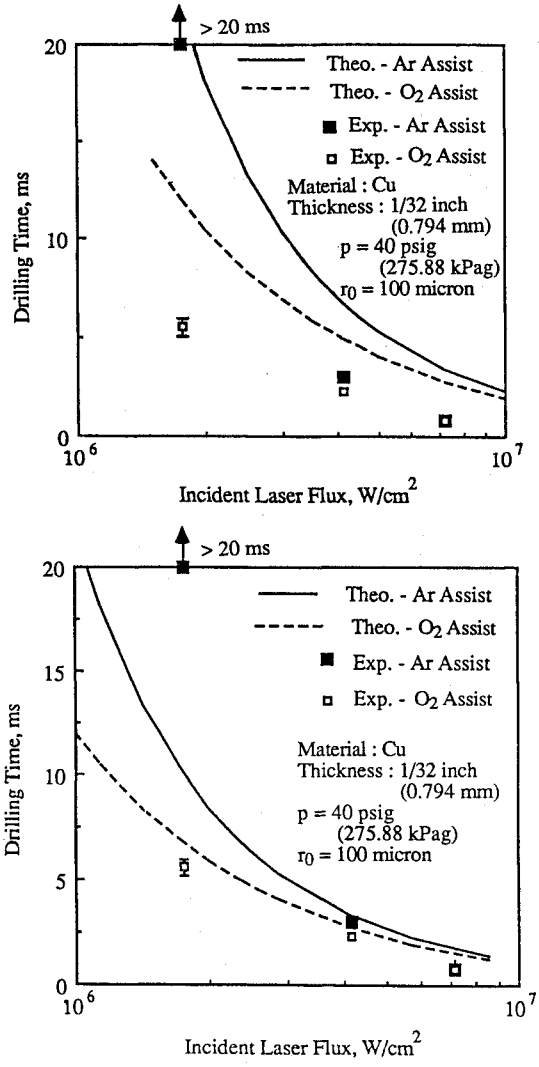

Fig. 9 Drilling time for 1/32-in. (0.794-mm) Cu: a) $\alpha_{Cu} = 0.02$; b) $\alpha_{Cu} = 0.35$.

The drilling time vs incident laser flux for the Al6061 sample is plotted in Fig. 8. Good quantitative as well as qualitative agreement between the theoretical and experimental data can be seen. The drilling time decreases as the incident power increases. It should be noted that the drilling time for the oxygen assist case happens to be longer than that for the argon case. Generally it is believed that the use of oxygen as an assist gas improves the efficiency of the process that would result in a lower drilling time for oxygen. But, as stated earlier, if the oxide melting point is significantly higher than the melting point of the metal, then a longer heating time is required to melt the oxide. Thus, the competing effects of change in the absorptivity of the surface due to oxide formation and the difference in the melting temperatures of oxide and metal determines whether or not the use of oxygen improves the process efficiency. Also, as the incident laser flux increases, the difference between the drilling times for argon and oxygen decreases, indicating that the role of the oxide becomes less important as the laser flux increases.

Results for Cu are plotted in Fig. 9a. The drilling times for the oxygen assist case are shorter than those for the argon assist case, indicating that, in the case of Cu, oxygen improves the efficiency of the process (unlike Al6061). The experimental value of the drilling time at the lowest power level using argon as an assist gas was not obtained because of the pulse width limitation of the laser (<20 ms). For copper, the quantitative agreement in the results is not as good as that for Al6061. However, it should be noted that better quantitative agreement could be obtained by properly adjusting the values of absorptivity used in the calculations. Figure 9b shows the results for Cu obtained by using $\alpha_{Cu} = 0.035$ for the argon assist case, instead of 0.02, which was used for the results for Fig. 9a. It can be seen that better quantitative agreement between the experimental and theoretical drilling time is generally obtained in Fig. 9b. However, the drilling time with argon at the lowest incident flux in Fig. 9b is significantly underpredicted. This is believed to be due to radial conduction, which was ignored in the analysis. Results for other metals also indicated that, for longer drilling times (>10 ms), which usually occurred at lower incident fluxes, the analysis tended to underpredict the drilling time.

When the analysis of this study is extended to samples that are thicker than those previously discussed, the drilling time is

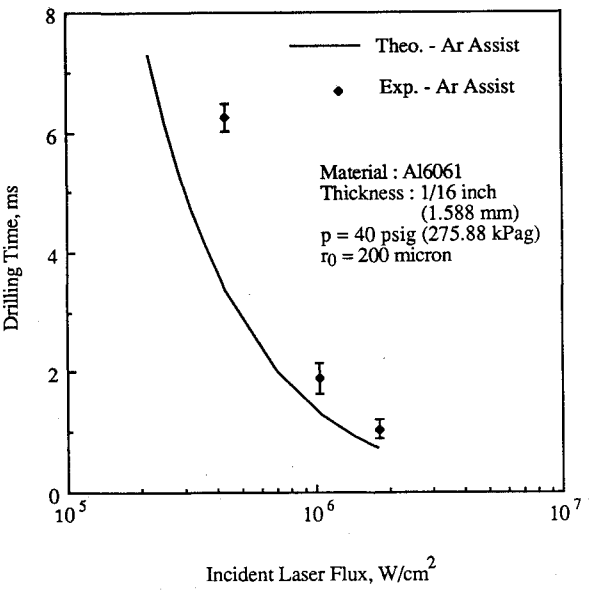

Fig. 10 Drilling time for 1/16 in. (1.588-mm) Al6061.

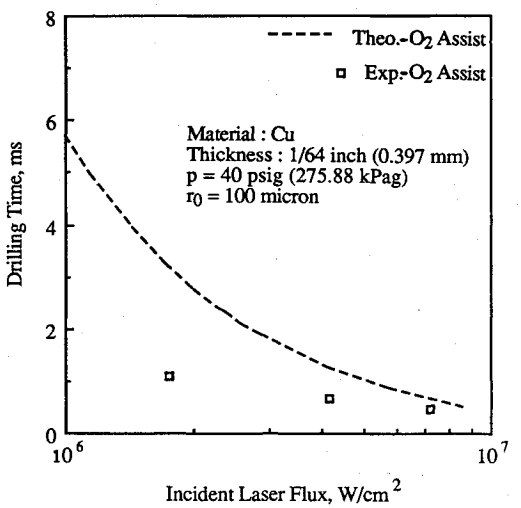

Fig. 11 Drilling time of 1/64-in. (0.397-mm) Cu ($\alpha_{Cu} = 0.035$).

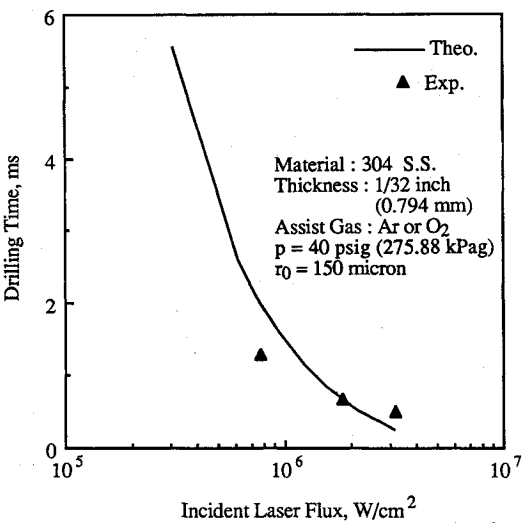

Fig. 12 Drilling time for 1/32-in. (0.794-mm) 304 stainless steel.

generally underpredicted. For example, Fig. 10 shows the results for thicker Al6061 samples (1/16 in. or 1.588 mm) with argon assist. It can be seen that the analysis underpredicts (by about 30–50%) the experimental drilling time. The underprediction of the drilling time is believed to be due to two factors. One factor is the neglect of the work necessary to expel molten material up out of the hole against gravity. As the hole depth increases (due to the increase in sample thickness), the molten material at the bottom of the hole needs to be driven up the sides of the hole by the assist gas in order to expel it. Since the model takes into account only the shearing of molten metal in the radial direction, the predicted drilling time is lower than the actual experimental value. The other factor is the neglect of flow penetration effects. The flow assumed in this study is stagnation flow over a flat surface. As the hole depth increases, the actual flow becomes more like a jet penetrating a hole than stagnation flow over a flat surface. To overcome these deficiencies in the model, the energy needed to drive the molten metal up the sides of the hole and the penetration of the gas flow could be taken into account. However, doing so would make the problem much more complex, demanding a more sophisticated solution, whereas the relatively simple analysis described here is a capable of predicting drilling times that are in reasonably good agreement with the experimental values (within the range of validity of the analysis).

When the analysis of this study is extended to samples that are thinner than those previously discussed, the drilling time is

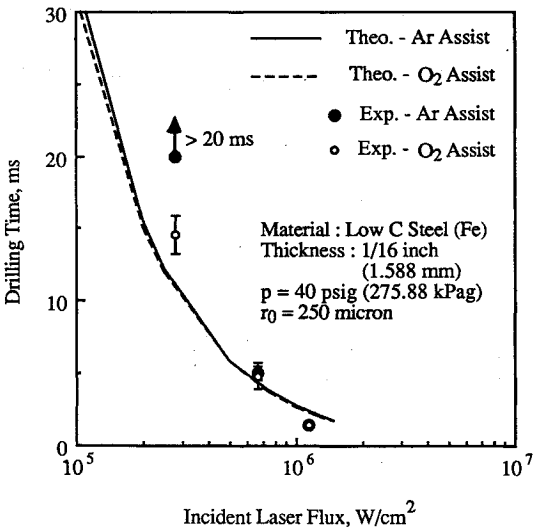

Fig. 13 Drilling time for 1/32-in. (0.794-mm) low-carbon steel.

generally overpredicted. For example, Fig. 11 shows the results of thinner Cu samples (1/64 in., or 0.397 mm) with oxygen assist. The drilling time is overpredicted (by about 1.5–3 times), as seen in Fig. 11. The overprediction of the drilling time in this case is a result of the fact that the semi-infinite solid assumption of the heat transfer problem is not valid for the thinner samples. This problem might be corrected by relaxing the quasisteady-state assumption of the model and solving the unsteady one-dimensional heat transfer and two-dimensional axisymmetric fluid flow equations with a finite boundary condition in the solid region. The resulting equations for the model would be considerably more complex, and a more sophisticated numerical solution would be required. Alternatively, acceptable results may be obtained for the case of "thin" samples from a simple one-dimensional, unsteady heat-conduction model, neglecting fluid flow and the molten metal shearing mechanism. [In this context a thin sample is one for which the conduction length scale ($\sqrt{4\kappa t}$) is of the order of or greater than the solid region thickness ($H-L$), where t is the drilling time.]

Results for 304 stainless steel are plotted in Fig. 12. For 304 stainless steel the drilling time for argon and oxygen are not much different, which agrees with the experimentally observed result. Also, the theoretical results for 304 stainless steel are in reasonably good quantitative agreement with the experimental results. Figure 13 shows the results for low-carbon steel. The drilling time for 1/16-in.- (1.588-mm-) thick low-carbon steel at low-incident laser flux is underpredicted, as seen in Fig. 13. The reasons for the discrepancy are believed to be the same as those already stated earlier for 1/16-in.- (1.588-mm-) thick Al6061 as well as radial conduction effects.

Conclusions

A steady-state model of the material removal by a gas jet during laser-metal interaction is described. The experimentally observed effects of change in absorptivity and change in temperature required to expel the molten metal are incorporated in the model. Results of drilling time are obtained for aluminum, copper, 304 stainless steel, and low-carbon steel. For an absorbed laser flux of the order of 10^4 W/cm^2, the liquid layer thickness is of the order of 10 μ, but it becomes of the order of 100 μ as the absorbed flux is increased to the order of 10^5 W/cm^2. Results for aluminum and copper showed that for absorbed laser fluxes of about $2\text{–}3 \times 10^5$ W/cm^2 the surface temperature exceeds the boiling point of the metal. Therefore, the gas-assisted molten metal expulsion mechanism would be expected to be valid up to these flux levels. The melting front

velocity also increases as the absorbed laser flux at the surface increases.

Reasonably good qualitative and quantitative agreement for drilling time between the experimental and theoretically calculated drilling times is obtained as long as the model assumptions are satisfied. The drilling time is observed to decrease with an increase in incident laser flux. It is also observed that the use of oxygen as an assist gas does not necessarily always improve the process efficiency. If a weakly absorbing oxide is formed that has a high melting point relative to that of the metal, then the use of oxygen tends to increase the drilling time. On the other hand, if a strongly absorbing oxide with a melting point similar to that of the metal is formed, then the use of oxygen tends to decrease the drilling time. In either case, the increase in absorptivity associated with the oxide formation and the difference in the melting points of oxide and metal seems to have more pronounced effect at lower values of incident flux. At higher values of laser incident flux ($>2\text{-}3\times10^6$ W/cm^2), the role of the oxide appears to be less important, as evidenced by the negligible difference between the drilling times for the oxygen-assisted case and the argon-assisted case.

Because of the assumptions used, the applicability of the model is restricted to sample thicknesses between 0.6 and 1.2 mm. For samples thinner than 0.6 mm, the drilling time is overpredicted because the semi-infinite solid assumption is not satisfied. It should be pointed out that this lower limit (0.6 mm) on sample thickness depends on the thermal diffusivity of metal and, therefore, will vary to a certain extent for different metals. For samples thicker than 1.2 mm, the drilling time is underpredicted because flow penetration and radial conduction effects are neglected.

Acknowledgment

Support for this work from the National Science Foundation (Grant CBT 86-96162) is gratefully acknowledged.

References

[1]Chun, M. K., and Rose, K., "Interaction of High Intensity Laser Beams with Metals," *Journal of Applied Physics.*, Vol. 41, No. 2, Feb. 1979, pp. 614–620.

[2]Schuocker, D., and Abel, W., "Material Removal Mechanism of Laser Cutting," *Proceedings of SPIE,* Vol. 455, Society of Photo-Optical Instrumentation Engineers, Bellingham, WA, 1983, pp. 88–95.

[3]Chan, C. L., and Mazumder, J., "One-Dimensional Steady-State Model for Damage by Vaporization and Liquid Expulsion Due to Laser-Material Interaction," *Journal of Applied Physics,* Vol. 62, No. 11, Dec. 1987, pp. 4579–4586.

[4]Duley, W. W., and Gonsalves, J. N., "CO_2 Laser Cutting of Thin Metal Sheets with Gas Jet Assist," *Optics and Laser Technology,* April 1974, pp. 78–81.

[5]White, F. M., *Viscous Fluid Flow,* McGraw-Hill, New York, 1974, pp. 675–678.

[6]Carslaw, H. S., and Jaeger, J. C., *Conduction of Heat in Solids,* 2nd ed., Clarendon, Oxford, UK, 1959, p. 75.

[7]Brades, E. A., (ed.), *Smithells Metals Reference Book,* 6th ed. Butterworths, London, 1981, Chap. 14.

[8]Zucrow, M. J., and Hoffman, J., *Gas Dynamics,* Vol 1, Wiley, New York, 1976, p. 192.

[9]Patel, R. S., and Brewster, M. Q., "Heat Transfer in Gas Assisted Laser-Metal Drilling: Experiment Results," *Journal of Themophysics and Heat Transfer*, Vol. 5, No. 1, 1991.

[10]Patel, R. S., and Brewster, M. Q., "Effect of Oxidation and Plume Formation on Low Power Nd-YAG Laser Metal Interaction," *Journal of Heat Transfer*, Vol. 112, Feb. 1990, pp. 170–177.

[11]Touloukian, Y. S., and Dewitt, D. P., "Thermal Radiative Properties, Nonmetallic Solids," *Thermophysical Properties of Matter,* IFI/Plenum Data, New York, 1972.